IEEE Access
Multidisciplinary | Rapid Review | Open Access Journal

Received December 19, 2020, accepted January 3, 2021, date of publication January 6, 2021, date of current version January 14, 2021.

Digital Object Identifier 10.1109/ACCESS.2021.3049513

Robust Active Contour Model Using Patch-Based Signed Pressure Force and Optimized Fractional-Order Edge

HONGLI LV[1,2], FANGJIAN ZHANG[1], AND RENFANG WANG[2,3]

[1]School of Information Technology, Shangqiu Normal University, Shangqiu 476000, China
[2]College of Big Data and Software Engineering, Zhejiang Wanli University, Ningbo 315100, China
[3]College of Computer Science and Artificial Intelligence, Wenzhou University, Wenzhou 325035, China

Corresponding author: Renfang Wang (renfang_wang@126.com)

This work was supported in part by the Key Scientific Research Projects of Higher Education Institutions of Henan Province under Grant 21A520037, in part by the Natural Science Foundation of Zhejiang Province under Grant LY20F020005, in part by the Project of the Science and Technique Plan for Ningbo Municipal under Grant 2019A610108, in part by the National Natural Science Foundation of China under Grant 2018YFB1004904, in part by the Plan Project of Wenzhou Municipal Science and Technology under Grant G20180036, and in part by the Project of the Science and Technology Plan for Zhejiang Province under Grant LGF19F020008 and LGF21F020023.

ABSTRACT Active contour models (ACMs) are the most widely used method for image segmentation. However, global fitting ACMs cannot effectively segment inhomogeneous images and local fitting ACMs suffer from noise and the initial position of the contour. To overcome these shortcomings, we propose a novel ACM that consists mainly of a local fitting term, an edge-based term and an external force term. The Jensen-Shannon divergence (JSD) based local fitting term is implemented to address intensity inhomogeneity. The edge-based term is formulated on Caputo-Fabrizio (CF) based fractional-order Gaussian derivatives and applied to compute the weighted area of the region inside the contour. The patch-based external force is designed to improve the robustness of the developed ACM to noise and the initial position of the contour. To further improve the robustness of the proposed model to noise, the input image is first replaced with its local robust statistics. Experimental results demonstrate that the developed model is not only robust to noise and the initial contour but also effective in dealing with intensity inhomogeneity.

INDEX TERMS Active contour, image segmentation, Jensen-Shannon divergence, fractional-order Gaussian derivatives, patch-based external force.

I. INTRODUCTION

Noise and intensity inhomogeneity make image segmentation a challenging task [1], [2]. To date, a large number of methods have been put forward to cope with these problems. Among these methods, the ACM is the most influential one. The basic idea of ACMs is that a predefined energy functional combining various image information is constructed and minimized to obtain the corresponding partial differential equation, which is utilized to drive the evolving curve towards the desired object boundaries [3], [4]. The most desirable advantage of ACMs is that sub-pixel accuracy of the target boundaries and a closed contour can be obtained [2], [5]. However, explicit ACMs have difficulty in dealing with the topological changes of the evolving curve [6].

The associate editor coordinating the review of this manuscript and approving it for publication was Kumaradevan Punithakumar.

The main advantage of implicit ACMs over explicit methods is the ability to automatically change the topology [5]. Therefore, this paper focuses mainly on implicit ACMs, namely, ACMs in the level set framework. In these ACMs, the evolving curve is implicitly represented as the zero level set of a high-dimensional function, which is called the level set function (LSF), and then the LSF is deformed according to the evolution equation [3], [4], which is obtained via a variational level set method. Generally, most of the existing ACMs can be classified into two classes: edge-based models [7]–[10] and region-based models [11]–[16]. The edge information of an image (e.g., the image gradient) is typically used by edge-based models to guide the evolving curve towards the desired boundaries of the target objects. In practice, these models are not only struggle to detect weak boundaries but also are highly sensitive to noise.

Region-based models use a certain region descriptor defined by image statistical information to guide the curve evolution. In general, the performance of region-based models is superior to that of edge-based models because of their antinoise property and ability to process weak boundaries. Among the region-based ACMs, one of the most popular global fitting methods is the Chan-Vese (CV) model [12], which replaces the piecewise smooth function of the well-known Mumford-Shan (MS) model [11] with the piecewise constant. The CV model has good performance on images with two homogeneous regions, but it fails to segment images with intensity inhomogeneity, because it relies only on global image information. The selective binary and Gaussian filtering regularized level set (SBGFRLS) model [13] uses the defined signed pressure force (SPF), which is formulated as the difference between the input image and the average of two global centers originating from the CV model. The SPF can be seen as an adaptive edge stopping function, which encourages the evolving curve to move towards the boundaries of the target objects. To reduce the influence of the interference regions, Han and Wu [14] propose a global median image fitting method with adaptive weight defined by the within-cluster absolute difference. To tackle the local minimization problem, a convex fuzzy ACM [15] integrated with a membership function is proposed. Based on [15], an improved global fuzzy ACM that uses the kernel metric is proposed. Similar to the CV model, these global fitting ACMs can effectively cope with homogeneous images, but they are not suitable for processing images with intensity inhomogeneity.

Based on local intensity information, many efficient local fitting models have been proposed to overcome the drawbacks of the global fitting methods. A popular one is the local binary fitting (LBF) model [17], [18], where a Gaussian kernel function is utilized for capturing the local information. In addition, Zhang *et al.* propose a local image fitting LIF) model [19], which assumes that the original image can be well approximated by the corresponding local fitted image (LFI) defined as the weighted average of two local fitting functions. A local region-based Chan-Vese model [20] that replaces the two global centers in the CV model with the corresponding local approximation functions in the LBF model is proposed. In [21]–[23], Kullback-Leibler divergence (KLD) is utilized to measure the difference between the original image and its LFI. Generally, local region-based methods perform well on inhomogeneous images when the initial contour is placed in an appropriate position. However, they suffer from noise and the initial position of the contour, which affect the quality of the final segmentation results.

To cope with intensity inhomogeneity and enhance the robustness of the model to noise and the initial contour, many hybrid ACMs have been proposed in the literature. Ali *et al.* [24] propose a hybrid ACM based on multiplicative and difference images. In [25], the global fitted image is applied to improve the performance of the LIF model. In [26]–[31], local and global SPFs are integrated into the methods through a adaptive weighting factor. Fang *et al.* [32] propose a hybrid ACM for medical image segmentation by synthesizing the global information and the local information. In the local CV model [33], the global term originates from the CV model, and the local term is constructed on the difference image, which is defined as the difference between the original image and the Gaussian smooth version. In [34], the global image characteristic is learned by self-organising maps and used to define the local fitting term. Sun *et al.* [35] propose a global fitting image based SPF to improve the robustness of the LIF model. By characterizing the fitting of global and local Gaussian distributions, Zhou *et al.* [36] propose a hybrid fitting energy framework. In these hybrid ACMs, the global and local fitting energy terms play different roles in image segmentation. The former can effectively improve the robustness of the model to the initial contour and noise. The latter is the key to dealing with inhomogeneous images.

To effectively segment noisy and inhomogeneous images, this paper presents a novel ACM, which is driven by the patch-based SPF, edge-based energy and JSD-based local fitting energy. First, local robust statistics are utilized to smooth the input image and reduce the effect of noise. Second, CF-based fractional-order Gaussian derivatives are used to extract the underlying edges of the target objects. To further suppress artifacts in the background, an energy functional is minimized to obtain the optimized fractional-order edge (FoE). The edge-based energy term is constructed to compute the weighted area of the region inside the contour. Third, we use image patches to define two global centers of image intensity and further define a novel SPF, which is used as the external force term. The newly proposed SPF can enhance the robustness of the model to noise and the initial contour to some extent. Finally, the local fitting energy term is formulated on the JSD, which is used to measure the difference between the smoothed image and its LFI. Experimental results on real and synthetic images demonstrate that the developed model can not only efficiently segment noisy and inhomogeneous images, but also accurately extract the boundaries of the objects of interest with more flexible initialization.

In summary, the main contributions of the paper are three-fold:

- The optimized FoE can extract the underlying boundaries of the objects of inerest and suppress artifacts in the background.
- We use image patches to define the external force term, which allows the proposed model to initialize the evolution curve in a more flexible way.
- The JSD is used to measure the difference between the smoothed image and its LFI. The proposed local fitting energy term enables the proposed model to segment inhomogeneous images.

The remainder of this paper is organized as follows. In Section II, we briefly review several related work on image segmentation and indicate their limitations. The model

proposed in this paper is introduced in detail in Section III. Section IV presents the experimental results to demonstrate the effectiveness of the proposed model. In SectionV, we discuss the proposed model. Finally, brief conclusions are drawn in Section VI.

II. RELATED WORK

A. THE CV MODEL

Based on the famous Munford-Shah model [11], Chan and Vese [12] propose a classic global fitting ACM with the assumption that the input image is formed by two regions of approximately piecewise constant intensities. The CV model can be expressed as the minimization of the following energy functional

$$\begin{aligned} E^{CV}(\phi(x), c_1, c_2) = \mu \cdot \int_\Omega \delta_\varepsilon(\phi(x))|\nabla\phi(x)|dx \\ + \lambda_1 \int_\Omega |I(x) - c_1|^2 M_1(\phi(x))dx \\ + \lambda_2 \int_\Omega |I(x) - c_2|^2 M_2(\phi(x))dx \end{aligned} \quad (1)$$

where μ, λ_1 and λ_2 are positive constants. $I(x)$ is the intensity of the variable x, which presents a point in the image domain Ω. ∇ is the gradient operator. $M_1(\phi(x)) = H_\varepsilon(\phi(x))$, $M_2(\phi(x)) = 1 - H_\varepsilon(\phi(x))$, and the smoothed Heaviside function $H_\varepsilon(\cdot)$ is given by

$$H_\varepsilon(z) = \frac{1}{2}\left(1 + \frac{2}{\pi}\arctan\left(\frac{z}{\varepsilon}\right)\right), \quad z \in \mathbb{R}. \quad (2)$$

$\delta_\varepsilon(z)$ is the Dirac function and the corresponding derivative of $H_\varepsilon(z)$. ε is a small fixed positive parameter. The LSF $\phi(x)$ can be expressed by

$$\begin{cases} \phi(x) = 0, & x \in \Omega \\ \phi(x) < 0, & x \in inside(C) \\ \phi(x) > 0, & x \in outside(C) \end{cases} \quad (3)$$

Keeping the LSF $\phi(x)$ fixed and minimizing the energy functional (1) with respect to c_1 and c_2, we have

$$c_i = \frac{\int_\Omega I(x)M_i(\phi(x))dx}{\int_\Omega M_i(\phi(x))dx}, \quad i = 1, 2 \quad (4)$$

From (4), we can find that the constants c_1 and c_2 can be seen as approximations of the image intensities outside and inside the contour C, respectively. The CV model performs well on images with weak boundaries or noise and does not suffer from the problem of initialization. However, c_1 and c_2 are related to the global properties of the image intensity, which makes the CV model suitable only for homogeneous images. For inhomogeneous images, c_1 and c_2 will not be accurate. Therefore, the CV model will obtain incorrect segmentation results on images with intensity inhomogeneity.

B. THE LBF MODEL

The LBF model [17], [18] is a local fitting ACM. A Gaussian kernel function is used to capture the local information of the image, which is utilized to address intensity inhomogeneity and embedded in the variational level set framework, that is,

$$\begin{aligned} &E^{LBF}(\phi(x), f_1(x), f_2(x)) \\ &= \lambda_1 \int_\Omega \left[\int_\Omega K_\sigma(x-y)|I(y) - f_1(x)|^2 M_1(\phi(y))dy\right]dx \\ &\quad + \lambda_2 \int_\Omega \left[\int_\Omega K_\sigma(x-y)|I(y) - f_2(x)|^2 M_2(\phi(y))dy\right]dx \end{aligned} \quad (5)$$

where λ_1 and λ_2 are fixed positive constants. K_σ is the Gaussian kernel function with standard deviation σ. $f_1(x)$ and $f_2(x)$ are two smooth functions.

Keeping $\phi(x)$ fixed and minimizing the energy functional (5) with respect to $f_1(x)$ and $f_2(x)$, we can obtain the following equations

$$f_i(x) = \frac{\int_\Omega K_\sigma(x-y)I(y)M_i(\phi(y))dy}{\int_\Omega K_\sigma(x-y)M_i(\phi(y))dy}, \quad i = 1, 2 \quad (6)$$

Obviously, $f_1(x)$ and $f_2(x)$ are computed in a local window and represent the local weighted averages of the image intensity. In this way, the LBF model can effectively deal with intensity inhomogeneity and generally obtains desirable results. However, the main drawback of the LBF model is that an appropriate position of the initial contour cannot be easily obtained.

C. THE LIF MODEL

In [19], Zhang *et al.* propose a local image fitted energy functional, which aims to minimize the difference between the LFI and the input image. The energy functional is given by

$$E^{LIF}(\phi(x)) = \frac{1}{2}\int_\Omega |I(x) - I^{LFI}(x)|^2 dx \quad (7)$$

and the LFI is defined by

$$I^{LFI}(x) = M_1(\phi(x))f_1(x) + M_2(\phi(x))f_2(x) \quad (8)$$

where $f_1(x)$ and $f_2(x)$ are the local intensity means inside and outside the contour.

The LIF model can effectively handle images with inhomogeneity. However, it is still sensitive to the initial contour. However, the Gaussian filtering based regularization method makes the computing cost less than that of the LBF model.

D. THE SBGFRLS MODEL

Zhang *et al.* [13] present the SBGFRLS model, which takes advantages of the region-based model [12] and the edge-based model [10]. Specifically, the edge stopping function in [10] is substituted by an SPF function, which is defined as

$$spf(I(x)) = \frac{I(x) - \frac{c_1+c_2}{2}}{max\left(\left|I(x) - \frac{c_1+c_2}{2}\right|\right)} \quad (9)$$

where $c_i (i = 1, 2)$ as defined in (4). The level set evolution equation is written as follows

$$\begin{aligned} \frac{\partial\phi}{\partial t} = spf(I(x))\left(div\left(\frac{\nabla\phi(x)}{|\nabla\phi(x)|}\right) + \alpha\right)|\nabla\phi(x)| \\ + \nabla spf(I(x)) \cdot \nabla\phi(x) \end{aligned} \quad (10)$$

where α is a constant velocity term, which is used to control the propagation speed of the LSF. To avoid the time-consuming re-initialization of the traditional methods, the SBGFRLS model uses the Gaussian filtering method to smooth the LSF after each iteration. Ignoring unnecessary terms, (10) can be simplified as

$$\frac{\partial \phi}{\partial t} = spf(I(x))\alpha|\nabla\phi(x)| \tag{11}$$

It can be seen that $spf(I(x))$ defined in (9) depends on the difference between the input image and the average of two global centers inside and outside the contour. Thus, the SBGFRLS model can deal with homogeneous images well. However, it is not ideal for segmenting images with intensity inhomogeneity.

III. PROPOSED MODEL

As discussed before, global fitting ACMs cannot effectively segment inhomogeneous images, and local fitting ACMs suffer from noise and the initial position of the contour. To overcome these shortcomings, in this subsection, we present a novel ACM in detail. Specifically, we first give the definition of the local robust statistics. Then, we present the FoE, which is optimized by an energy functional. Next, we define a novel patch-based SPF. Finally, the local statistical information of the input image is utilized to define the proposed local fitting term.

A. LOCAL ROBUST STATISTICS

As pointed out in [37], the local robust statistics, which consist of intensity median (*MED*), local interquartile range (*IQR*) and local mean absolute deviation (*MAD*), are insensitive to noise. Therefore, the local robust statistics of the input image are first computed to enhance the robustness of the developed model to noise. More explicitly, let N_x be a square window centered on x and $x_1, x_2, \cdots, x_m$ be an ascending intensities array in N_x, then $MED(x)$ is defined as the intensity median in the square window N_x, as shown

$$MED(x) = \begin{cases} x_{\frac{(i+1)}{2}}, & if\ i\ is\ odd \\ \frac{1}{2}(x_{\frac{i}{2}} + x_{(\frac{i}{2}+1)}), & if\ i\ is\ even \end{cases} \tag{12}$$

The distance between the first quartile and the third quartile is denoted as $IQR(x)$, which is expressed by

$$IQR(x) = Q_3(x) - Q_1(x) \tag{13}$$

where $Q_i(x)(i = 1, 3)$ represents the ith quartile of $x_1, x_2, \cdots, x_m$, respectively. The mean absolute deviation $MAD(x)$ is given as follows

$$MAD(x) = \frac{\sum_{i=1}^{m} |x_i - \bar{x}|}{m} \tag{14}$$

where m is the number of pixels in the local window N_x and $\bar{x}$ is the mean of $x_1, x_2, \cdots, x_m$. By integrating the above three features, we can define the local robust statistics of the input image as follows

$$I^{LRS}(x) = MED(x) + \tau_1 IQR(x) + \tau_2 MAD(x) \tag{15}$$

Numerically, the size of window N_x is fixed at 5×5, $\tau_1, \tau_2 \in [0, 1]$. The values of τ_1 and τ_2 should be selected according to the level of noise and intensity inhomogeneity. Generally, if the original image is homogeneous or corrupted by little noise, τ_1 and τ_2 should be set to low values, otherwise, they should be set to high values. In this paper, we set $\tau_1 = \tau_2 = 0.1$, which work well on all test images.

B. OPTIMIZED FRACTIONAL-ORDER EDGE

One of the famous second-order differentiation based edge detection operator is the Laplacian of Gaussian (LoG). However, the existence of the second-order derivative makes the LoG amplify all high-frequency components. Therefore, the LoG is sensitive to noise and inhomogeneous textures, and will introduce artifacts or false edges. Inspired by [5], [38], [39], we use the fractional-order Gaussian derivatives, which have closed-form solution according to the definition of CF derivative [40], to obtain the image edges.

The specific CF fractional-order derivative definition with the zero initial condition can be expressed as

$${}^{CF}D_t^{(v)} f(t) = \frac{1}{1-v}\int_0^t exp(-\frac{v}{1-v}(t-\tau))\partial_t f(t)|_{t=\tau} d\tau \tag{16}$$

where $v \in [0, 1)$. As suggested in [40], the generalized higher-order derivative, i.e., the $(n + v)$-order CF fractional derivative can be obtained easily via integration by parts as follows

$$\begin{aligned} {}^{CF}D_t^{(n+v)} f(t) = \frac{1}{1-v}\sum_{k=1}^{n}\left[\left(-\frac{v}{1-v}\right)^{n-k}\partial_t^k f(t)\right] \\ + \left(-\frac{v}{1-v}\right)^n {}^{CF}D_t^{(v)} f(t) \end{aligned} \tag{17}$$

where n is an integer and $v \in [0, 1)$.

For the normalized Gaussian function with mean μ and variance σ

$$G_{\mu,\sigma}(t) = \frac{1}{\sqrt{2\pi}\sigma} exp\left(-\frac{(t-\mu)^2}{2\sigma^2}\right) \tag{18}$$

its first derivative can be written as

$$\partial_t G_{\mu,\sigma}(t) = \frac{(t-\mu)}{\sqrt{2\pi}\sigma^3} G_{\mu,\sigma}(t) \tag{19}$$

By using the CF definition (16) and the method of integration by parts, we can obtain the following v-order fractional derivative of the Gaussian function in the left part

$$\begin{aligned} &{}^{CF}\underrightarrow{D}_t^v G_{\mu,\sigma}(t) \\ &= \frac{1}{1-v}\int_0^t exp\left(-\frac{v}{1-v}(t-\tau)\right)\partial_t G_{\mu,\sigma}(\tau) d\tau \\ &= \frac{1+\gamma_v}{\sqrt{2\pi}\sigma^3} exp\left(-\gamma_v\left(t-\mu-\frac{\sigma^2}{2}\gamma_v\right)\right)\zeta_{\mu,\sigma,v}(t) \end{aligned} \tag{20}$$

where $\gamma_v = v/(1-v)$ and

$$\begin{aligned}
&\zeta_{\mu,\sigma,v}(t) \\
&= \int_0^t (\mu-\tau) exp\left(-\frac{(\tau-(\mu+\gamma_v\sigma^2))^2}{2\sigma^2}\right) d\tau \\
&= \frac{\sqrt{2\pi}\sigma^3\gamma_v}{2}\left[erf\left(-\frac{\xi_{\mu,\sigma,v}}{\sqrt{2}\sigma}\right) - erf\left(-\frac{\xi_{\mu,\sigma,v}-t}{\sqrt{2}\sigma}\right)\right] \\
&\quad + \sigma^2\left[exp\left(-\frac{(t-\xi_{\mu,\sigma,v})^2}{2\sigma^2}\right) - exp\left(-\frac{\xi_{\mu,\sigma,v}^2}{2\sigma^2}\right)\right] \qquad (21)
\end{aligned}$$

where $erf(\cdot)$ is the error function and $\xi_{\mu,\sigma,v} = \mu + \gamma_v\sigma^2$.

Analogously, the v-order fractional derivative of the Gaussian function in the right part can be obtained as follows

$$\begin{aligned}
{}^{CF}\underset{\leftarrow}{D}_t^v G_{\mu,\sigma}(t) &= \frac{1}{1-v}\int_t^\infty exp\left(-\frac{v(t-\tau)}{1-v}\right)\partial_t G_{\mu,\sigma}(\tau)d\tau \\
&= \frac{\gamma_v+1}{\sqrt{2}} exp\left(-\frac{\mu^2-\xi_{\mu,\sigma,v}^2+2\gamma_v\sigma^2 t}{2\sigma^2}\right) \\
&\quad \times\left[-\frac{\gamma_v}{\sqrt{2}}\left(erf\left(\frac{\xi_{\mu,\sigma,v}-t}{\sqrt{2}\sigma}\right)+1\right)\right. \\
&\quad \left. -\frac{exp\left(-\frac{(\xi_{\mu,\sigma,v}-t)^2}{2\sigma^2}\right)}{\sqrt{\pi}\sigma}\right] \qquad (22)
\end{aligned}$$

According to (17), the $(n+v)$-order CF fractional derivative of the Gaussian function can be expressed by

$$\begin{aligned}
&{}^{CF}\underset{\rightarrow}{D}_t^{n+v} G_{\mu,\sigma}(t) \\
&= (-\gamma_v)^n\left[{}^{CF}\underset{\rightarrow}{D}_t^v G_{\mu,\sigma}(t)\right] \\
&\quad + (\gamma_v+1)\left[\sum_{k=1}^{n}(-\gamma_v)^{n-k}\partial_t^k G_{\mu,\sigma}(t)\right] \qquad (23)
\end{aligned}$$

and

$$\begin{aligned}
&{}^{CF}\underset{\leftarrow}{D}_t^{n+v} G_{\mu,\sigma}(t) \\
&= (-\gamma_v)^n\left[{}^{CF}\underset{\leftarrow}{D}_t^v G_{\mu,\sigma}(t)\right] \\
&\quad + (\gamma_v+1)\left[\sum_{k=1}^{n}(-\gamma_v)^{n-k}\partial_t^k G_{\mu,\sigma}(t)\right] \qquad (24)
\end{aligned}$$

The principle of the LoG is that the Gaussian filter is first used to smooth the image I and then the Laplacian operator is used to obtain the edge of the smoothed image. The LoG is written mathematically as

$$\nabla^2(G_{\mu,\sigma}(x,y) * I(x,y)) = \nabla^2 G_{\mu,\sigma}(x,y) * I(x,y) \qquad (25)$$

where $*$ denotes the convolution operator and ∇ is the gradient operator. Similar to the definition of the LoG, the proposed FoE can be obtain, as shown,

$$\begin{aligned}
FoE(x) &= {}^{CF}\nabla_{x,y}^{n+v}(G_{\mu,\sigma}(x,y) * I(x,y)) \\
&= {}^{CF}\nabla_{x,y}^{n+v} G_{\mu,\sigma}(x,y) * I(x,y) \qquad (26)
\end{aligned}$$

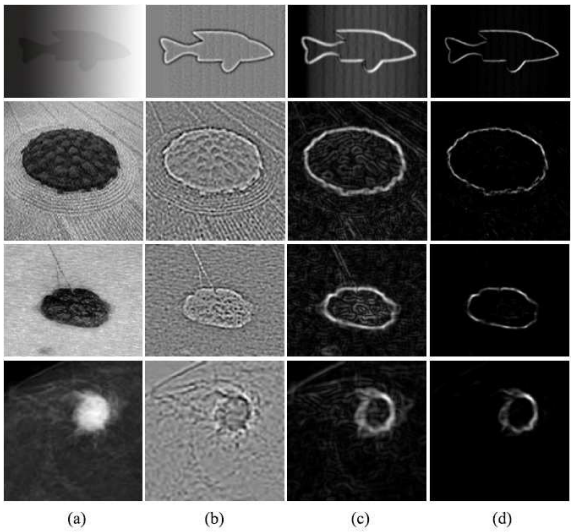

FIGURE 1. Effectiveness of the optimized FoE. (a) Original image, (b) LoG, (c) FoE, (d) Optimized FoE.

and the 1D convolution masks in the x and y directions are given as follows [36]

$${}^{CF}\nabla_x^{n+v} G_{\mu,\sigma}(x) = {}^{CF}\underset{\rightarrow}{D}_t^{n+v} G_{\mu,\sigma}(x) - {}^{CF}\underset{\leftarrow}{D}_t^{n+v} G_{\mu,\sigma}(x) \qquad (27)$$

$${}^{CF}\nabla_y^{n+v} G_{\mu,\sigma}(y) = {}^{CF}\underset{\rightarrow}{D}_t^{n+v} G_{\mu,\sigma}(y) - {}^{CF}\underset{\leftarrow}{D}_t^{n+v} G_{\mu,\sigma}(y) \qquad (28)$$

Inspired by [5], the optimized FoE is used to extract the object edges and suppress artifacts in the background. The optimized FoE is obtained by minimizing the following energy functional

$$\begin{aligned}
E(F(x)) = \int_\Omega &[g(|\nabla I(x)|)(F(x)-0)^2 \\
&+ (1-g(|\nabla I(x)|))(F(x)-FoE(x)]dx \qquad (29)
\end{aligned}$$

where Δ is the Laplace operator, $g(|\nabla I|) = exp(-k|\nabla G_\sigma * I|)$, k is a positive constant and $F(x)$ denotes the optimized FoE of the original image. In the homogeneous regions, $g(|\nabla I|)$ has a large value, which makes $F(x)$ close to 0. Moreover, the values of $g(|\nabla I|)$ are small at the locations near the boundaries of the objects of interest, which drives $F(x)$ towards $FoE(x)$. As shown in Fig. 1, the proposed optimized FoE can suppress artifacts in the background and provide more reliable results of the object boundaries compared with the LoG and FoE.

C. PATCH-BASED SPF

Based on the SPF proposed in [13], many improved versions [4], [26]–[31], [41], [42] have been proposed by using different strategies. However, they may have low robustness to noise because the spatial information of pixels is not considered. Inspired by [43], a patch-based SPF is defined to improve the robustness of the proposed model. Let N_x be the 5×5 neighborhood of pixel x and $P(x)$ be the corresponding

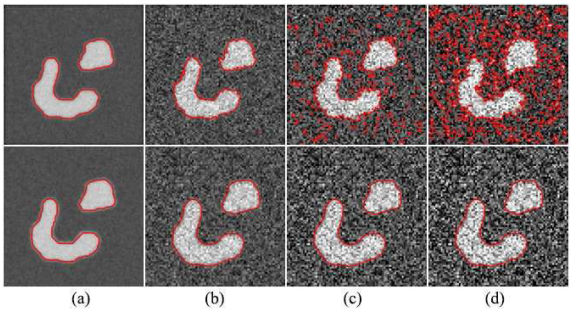

FIGURE 2. Robustness of the proposed *pspf*$(I(x))$. (a) Results of original image, (b)-(d) Results of images corrupted by Gaussian noise with levels of 0.01,0.03,0.05, respectively. Row 1: Results of the SBGFRLS model [13]. Row 2: Results of the proposed model (35).

image patch centered on x, $P_r(x)$ denotes the intensity of pixel $r \in N_x$, and $V_{ri}(i = 1, 2)$ denotes the intensity of pixel r in the i-th patch-based center $V_i(i = 1, 2)$, as shown

$$V_{ri} = \frac{\int_\Omega M_i(\phi(x))w_r(x)P_r(x)dx}{\int_\Omega M_i(\phi(x))w_r(x)dx}, \quad i = 1, 2 \tag{30}$$

where $w_r(x)$ is the weight associated with $P_r(x)$, which is given by

$$w_r(x) = \frac{\xi_r(x)}{\sum_{r\in N_x}\xi_r(x)} \tag{31}$$

Here,

$$\xi_r(x) = exp\left[-\left(\rho_r(x) - \frac{\sum_{r\in N_x}\rho_r(x)}{25}\right)\right] \tag{32}$$

and

$$\rho_r(x) = \left[\frac{\sum_{r'\in N_x\setminus\{r\}}(P_{r'}(x) - P_r(x))^2}{24}\right]^{1/2} \tag{33}$$

where $\rho_r(x)$ denotes the mean-square deviation of $P_r(x)$. Then, the proposed patch-based SPF is given by

$$pspf(I(x)) = \frac{mean\left(P(x) - \frac{V_1+V_2}{2}\right)}{max\left(\left|mean\left(P(x) - \frac{V_1+V_2}{2}\right)\right|\right)} \tag{34}$$

Obviously, the proposed SPF uses the information of the image patches to replace the intensity of pixels in the traditional SPFs. The weighting scheme assigns anisotropic weights to the pixels in each image patch. Therefore, the proposed *pspf*$(I(x))$ is more robust to noise. To demonstrate this, we use the following evolution equation to segment an image with different levels of Gaussian noise.

$$\frac{\partial\phi}{\partial t} = pspf(I(x))|\nabla\phi(x)| \tag{35}$$

It is worth noting that (35) is obtained only by replacing *spf*$(I(x))$ in the SBGFRLS model with the proposed *pspf*$(I(x))$. As shown in Fig. 2, the performance of the proposed model is much better than that of the SBGFRLS model in the case of severe noise.

Compared with other pixel-based SPFs [13], [26]–[31], [41], [42], the proposed *pspf*$(I(x))$ mainly has the following differences:

- The proposed *pspf*$(I(x))$ is defined by using the information of the image patches. Moreover, pixels in each image patch have anisotropic weights, which emphasize the degrees of their contribution to the patch-based centers. Therefore, the proposed *pspf*$(I(x))$ is more robust to noise.
- The purpose of most SPFs [13], [26]–[31], [41], [42] is to control the evolution speed of the curve. However, the proposed *psfp*$(I(x))$ can be seen as an external force term and is designed to tackle noise and the problem of the initial contour.
- Although the existing global-based SPFs are robust to noise and the initial contour to some extent, the level set evolution of the proposed model integrating the proposed *pspf*$(I(x))$ can start with a constant function, which is demonstrated in Section IV.

Notably, the ability of the proposed *pspf*$(I(x))$ to segment inhomogeneous images compared with local-based SPFs [26]–[28], [42] is still limited. To successfully segment images with intensity inhomogeneity, the local image characteristics must be considered.

D. LOCAL FITTING TERM

Taking the local image characteristics into consideration is the key to successfully segmenting inhomogeneous images. Similar to most models [17], [19], we assume that inhomogeneous images are local homogeneity and can be well approximated by their LFIs. As mentioned above, models [21]–[23] use the KLD to measure the difference between the original image and its LFIs. However, the KLD does not satisfy the properties of a distance and is an asymmetric measure. In [44], the KLD is replaced by its symmetrization version, i.e., the Jeffreys divergence (JD). However, the JD and KLD are not upper bounded, while the JSD is symmetrical and always bounded. In addition, the square root of the JSD is a metric distance satisfying the triangular inequality [45]. Therefore, the JSD is chosen to construct the proposed local fitting term, which can be expressed as

$$E^L(\phi(x)) = \frac{1}{2}\int_\Omega\left[I^{LRS}(x)log\left(\frac{I^{LRS}(x)}{M(x)}\right) + M(x)log\left(\frac{M(x)}{I^{LRS}(x)}\right)\right]dx \tag{36}$$

and

$$M(x) = \frac{I^{LRS}(x) + I^{LFI}(x)}{2} \tag{37}$$

where $I^{LRS}(x)$ is defined in (15) and $I^{LFI}(x)$ is the LFI of $I^{LRS}(x)$.

E. EVOLUTION EQUATION OF THE PROPOSED MODEL

Incorporating the edge-based term and the length regularizing term into (36), we can obtain the following energy functional

$$E(\phi(x)) = \lambda E^L(\phi(x)) + \mu(E^E(\phi(x)) + E^{LR}(\phi(x))) \quad (38)$$

with

$$E^E(\phi(x)) = \int_\Omega F(x) H_\varepsilon(-\phi(x))dx \quad (39)$$

and

$$E^{LR}(\phi(x)) = \int_\Omega \delta_\varepsilon(\phi(x))|\nabla\phi(x)|dx \quad (40)$$

where λ and μ are fixed positive constants. $E^E(\phi(x))$ is and edge-based term that computes the weighted area of the region $\{x \in \Omega, \phi(x) < 0\}$, and $E^{LR}(\phi(x))$ is the length regularizing term, which can constrain the perimeter of the contour.

Keeping other variables fixed and minimizing the energy functional (38) with respect to the LSF ϕ, the following evolution equation can be obtained

$$\frac{\partial\phi}{\partial t} = \lambda e(x) + \mu\delta_\varepsilon(\phi)\left[F(x) + div\left(\frac{\nabla\phi}{|\nabla\phi|}\right)\right] \quad (41)$$

and

$$e(x) = \frac{1}{4}(f_1(x) - f_2(x))\left[\frac{I^{LRS}(x)}{M(x)} - 1 - log\left(\frac{M(x)}{I^{LRS}(x)}\right)\right] \quad (42)$$

The JSD-based local fitting term can effectively deal with intensity inhomogeneity, however, it still suffers from curve initialization and noise. By contrast, the patch-based SPF is not sensitive to the initial position of the contour, but it fails to segment inhomogeneous images. Therefore, it is necessary to incorporate them into one evolution equation. Thus, we obtain the following evolution equation

$$\frac{\partial\phi}{\partial t} = \lambda e(x) + \mu\delta_\varepsilon(\phi)\left[F(x) + div\left(\frac{\nabla\phi}{|\nabla\phi|}\right)\right] + \nu pspf(I(x)) \quad (43)$$

where $\lambda > 0$, $\mu > 0$ and $\nu > 0$ are weighting parameters, which are used to adjust the effects of each term of the proposed model. It is worth noting that $psfp(I(x))$ in (43) is used as an adaptive external force. This is different from other models [13], [26]–[28], [38], [39], the SPFs of which are used to control the evolution speed of the curve. The external force $psfp(I(x))$ makes the proposed model more robust to noise and the initial contour, but also makes the level set evolution of the proposed model start with a constant value function.

F. ALGORITHM IMPLEMENTATION

To solve the (43), a finite difference method is used. Let $A(\phi^k)$ be the right side of (43) after the k-th iteration, then the $(k+1)$-th iteration of the LSF ϕ can be obtained by

$$\phi^{k+1} = \phi^k + \Delta t \cdot A(\phi^k) \quad (44)$$

After each iteration, we use the Gaussian filter to regularize the LSF as follows

$$\phi^{k+1} = G_\varsigma * \phi^{k+1} \quad (45)$$

where ς is the standard deviation of the Gaussian kernel function and fixed to 0.3 in all experiments. In addition, if the condition $err = ||\phi^{k+1} - \phi^k||_F / ||\phi^k||_F \leq tol$ or the number of iterations reaches the maximum number of iterations $Iter_{max}$, then the iteration process conducted by (44) is terminated. In this paper, tol and $Iter_{max}$ are experimentally set as 0.001 and 2000, respectively. The main steps of the proposed model are organized in Algorithm 1.

Algorithm 1 Algorithm Steps of the Proposed Model

Input: σ, Δt, λ, μ, ν, $Iter_{max}$, tol
Output: ϕ
Initialize the LSF by (3);
Compute I^{LRS} by (15);
Compute $F(x)$ by (29);
while $k \leq Iter_{max}$ **do**
  Computer $V_i(i = 1, 2))$ by (30);
  Computer $pspf(x)$ by (34);
  Computer $f_i(i = 1, 2))$ by (6);
  Update ϕ by (44);
  Regularize the LSF by (45);
  If $err \leq tol$
    break;
  end
end

IV. EXPERIMENTAL RESULTS

In this section, the proposed model is tested on both synthetic and real images, and it is implemented in MATLAB R2019b on a 2.6GHz Intel (R) Core (TM) i7 personal computer. The parameters of the proposed model are chosen based on experience or experiment and fixed as $\lambda = 4$, $\nu = 0.05$, $\sigma = 3$ (the standard deviation of the Gaussian kernel in (7) used to control the size of the local window) and $\Delta t = 1$ for all the experiments in this section. However, μ is set according to the image intensity property. The segmentation results of the proposed model are compared with those of global fitting models (CV [12] and SBGFRLS [13]), local fitting models (LBF [17] and LIF [19]), and hybrid models (GLSEPF [28], ALGR [29], FRAGL [30] and HLFRA [31]). The parameters of the compared methods are set as the values described in the original papers.

To evaluate the results, the segmentation accuracy of different models is quantitatively assessed by using the Dice similarity coefficient (DSC) [13], as shown

$$DSC(G, T) = \frac{2 \times |G \bigcap T|}{|G| + |T|} \quad (46)$$

where G is the ground-truth segmentation. T denotes the corresponding segmentation results of different methods.

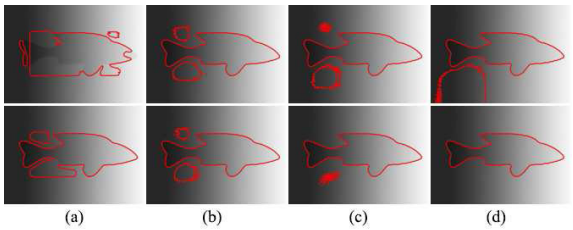

FIGURE 3. Contribution of edge-based term. (a)-(d): Results after 10, 50, 150, 300 iterations. Row 1: edge-based term is removed. Row 2: edge-based term is reserved.

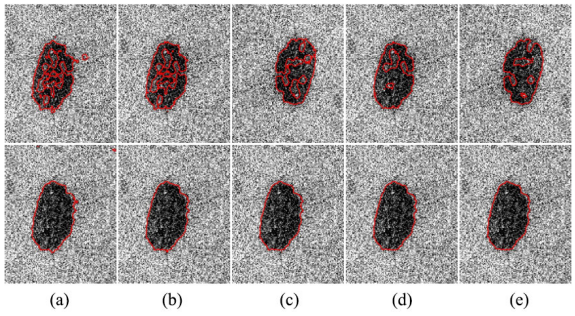

FIGURE 4. Contribution of the external force term $pspf(I(x))$. (a)-(e): Segmentation results by setting parameter μ as 1,3,5,7,9, respectively. Row 1: $pspf(I(x))$ is removed. Row 2: $pspf(I(x))$ is reserved.

$|\cdot|$ represents the pixel number of the regions G, T or $G \bigcap T$. Obviously, $DSC \in [0, 1]$, where a the larger value of the DSC means that a better segmentation result is obtained.

A. RESULTS OF THE PROPOSED MODEL

In this subsection, some experiments are performed to show the effectiveness of the proposed model. We first demonstrate the contribution of the edge-based term, which is used to compute the weighted area of the contour. Rows 1 and 2 of Fig. 3 show the process of the level set evolution without the edge-based term and with the edge-based term, respectively. As shown in Fig. 3, the edge-based term can accelerate the convergence speed of the level set evolution and helps in obtaining the correct segmentation results. Therefore, the edge-based term is reserved in the following experiments.

As mentioned above, the proposed patch-based SPF $pspf(I(x))$ is used as an external term, which can enhance the robustness of the proposed model to noise. To show this, Gaussian noise is added to a skin lesion image, the variance of which is set as 0.05 by the MATLAB function *imnoise*. Row 1 of Fig. 4 shows the segmentation results of the proposed model without the external term by setting the parameter μ as 1, 3, 5, 7, and 9. We can find that the segmentation results are not ideal. In fact, no matter how we adjust the parameter μ, correct segmentation results cannot be obtained in this case. By contrast, reserving the external term can yield desirable results, as shown in row 2 of Fig. 4. Therefore, the patch-based external term is necessary for the developed model to successfully segment noisy images.

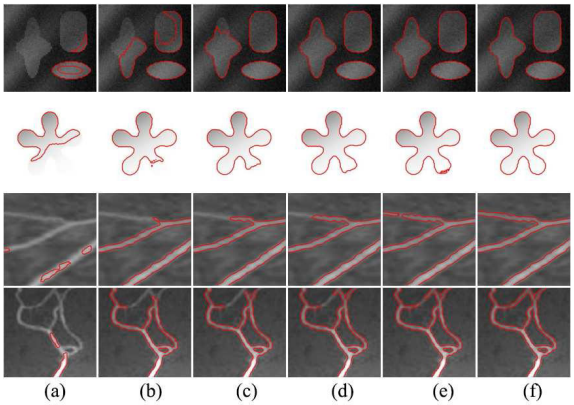

FIGURE 5. Effectiveness of the level set evolution starting with constant function. (a)-(f): Results after 10,50,100,150,200,250 iterations, respectively.

Local fitting ACMs always suffer from the position of the initial contour. An improper location will lead to incorrect segmentation results. To enhance the robustness of the proposed model to the initialization of the contour, a novel patch-based SPF is defined that can make the level set evolution of the proposed model start with a constant function. In the following experiment, the LSF is set as $\{\phi(x) = 1, x \in \Omega\}$ and four images are tested to assess the effectiveness of the constant value initialization method. Specifically, the images shown in row 2 are corrupted by severe intensity inhomogeneity. From row 1 to row 4, the parameter μ is set as 0.6, 0.01, 0.3 and 0.25, respectively. Fig. 5(a)-(f) show the segmentation results after 10, 50, 100, 150, 200 and 250 iterations, respectively. From the process of the level set evolution, we can find that the obtained segmentation results are becoming increasingly more accurate. The final segmentation results are shown in Fig. 5(f). This experiment shows that desirable results can be obtained when the LSF is initialized to a constant function.

B. COMPARISONS WITH POPULAR ACMs

In the following experiments, two widely used vessel images with intensity inhomogeneity are used to evaluate the robustness of the developed model and several other methods. The parameter μ of the proposed model is set as 0.3. Figs. 6(a) and 7(a) show original images with different initial contours. In (b)-(j) of Figs. 6 and 7, the segmentation results of the CV, SBGFRLS, ALGR, FRAGL, HLFRA, LBF, LIF, GLSEPF and proposed model are shown, respectively. We can observe that the global fitting based CV and SBGFRLS methods cannot obtain desirable segmentation results for inhomogeneous images. The main reason is that their energy functional integrates only the global information of each image, which cannot effectively represent the local feature of inhomogeneous images. Moreover, the positions of the initial contour are different, but the CV and SBGFRLS methods yield similar segmentation results. Therefore, we can conclude that they are insensitive to the initial contour to

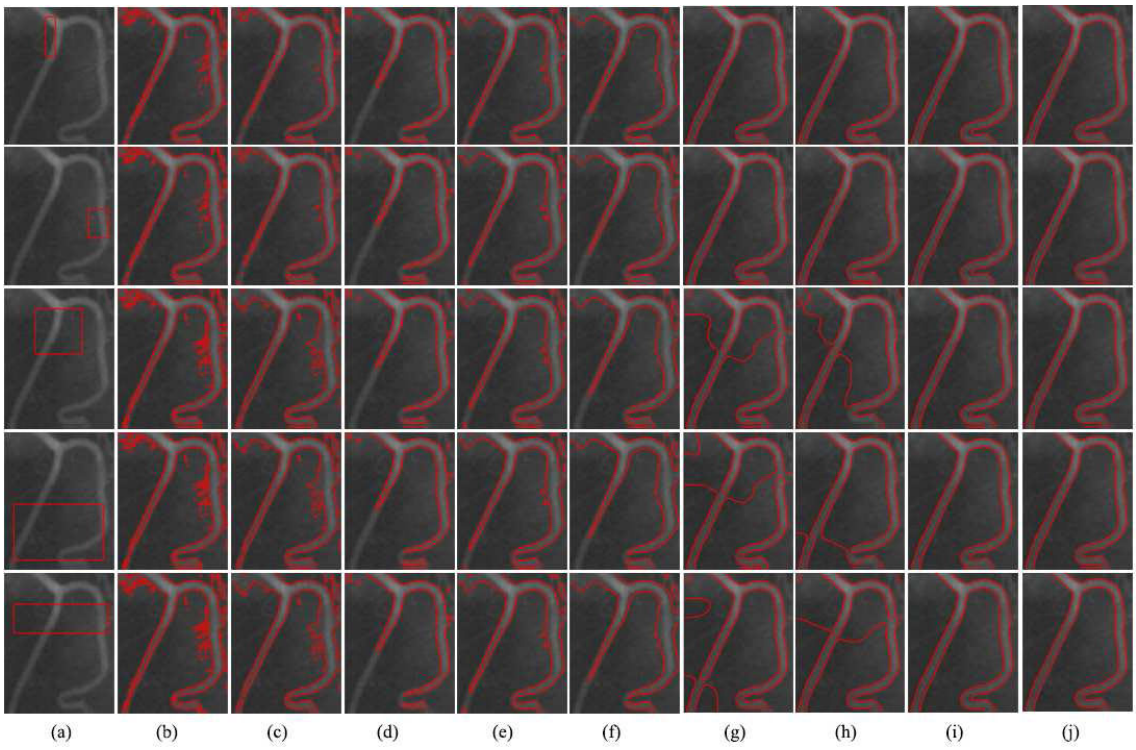

FIGURE 6. Segmentation results with different initial contours. (a) Original image with different initial contours, (b)-(j) Results of CV, SBGFRLS, ALGR, FRAGL, HLFRA, LBF, LIF, GLSEPF and the proposed model, respectively.

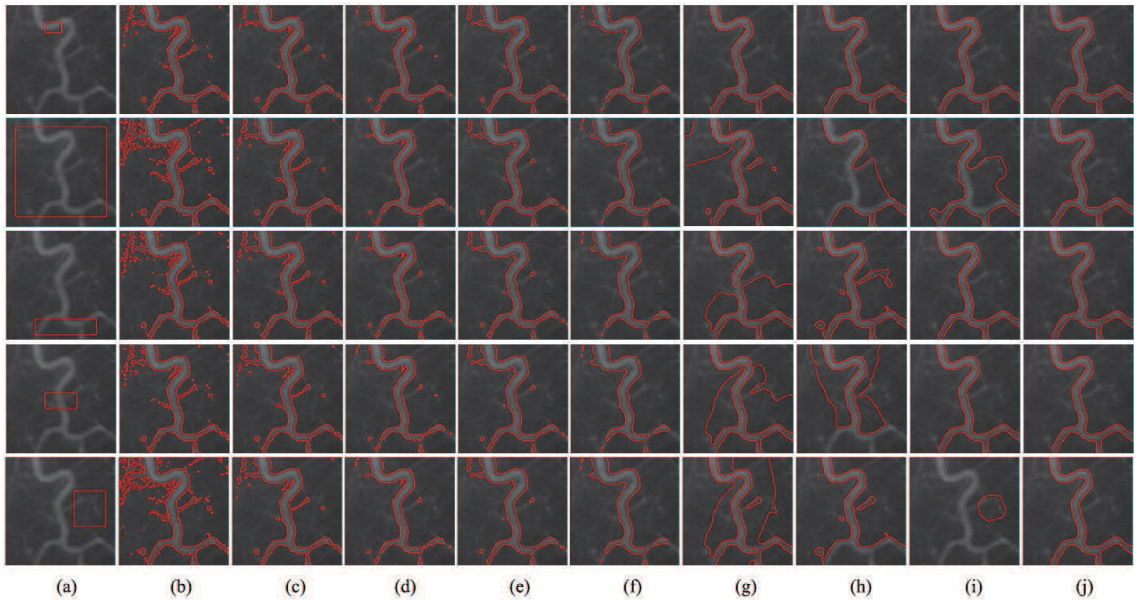

FIGURE 7. Segmentation results with different initial contours. (a) Original image with different initial contours, (b)-(j) Results of CV, SBGFRLS, ALGR, FRAGL, HLFRA, LBF, LIF, GLSEPF and the proposed model, respectively.

some extent. Local fitting based LBF and LIF can achieve desirable performances, as shown in rows 1 and 2 of Fig. 6 and row 1 of Fig. 7. However, their performances are worse in other situations. This demonstrates that local fitting based ACMs can cope with intensity inhomogeneity, but they are sensitive to the position of the initial contour. Even though the ALGR, FRAGL and HLFRA methods integrate local information based SPF into the models, they fail to deal with intensity inhomogeneity. By contrast, GLSEPF and our model perform better, as shown in Fig. 6. However, compared

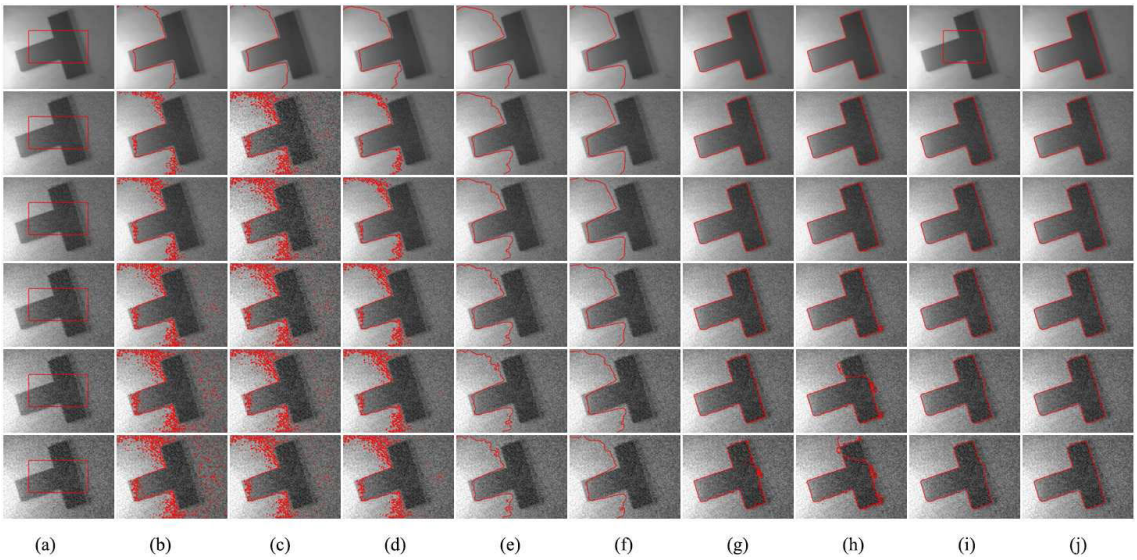

FIGURE 8. Segmentation results of the image with different levels of Gaussian noise. (a) Images with initial contour, (b)-(j) Results of CV, SBGFRLS, ALGR, FRAGL, HLFRA, LBF, LIF, GLSEPF and the proposed model, respectively. Rows 1 to 6: Images with noise level 0, 0.0005, 0.001, 0.002, 0.003, 0.004.

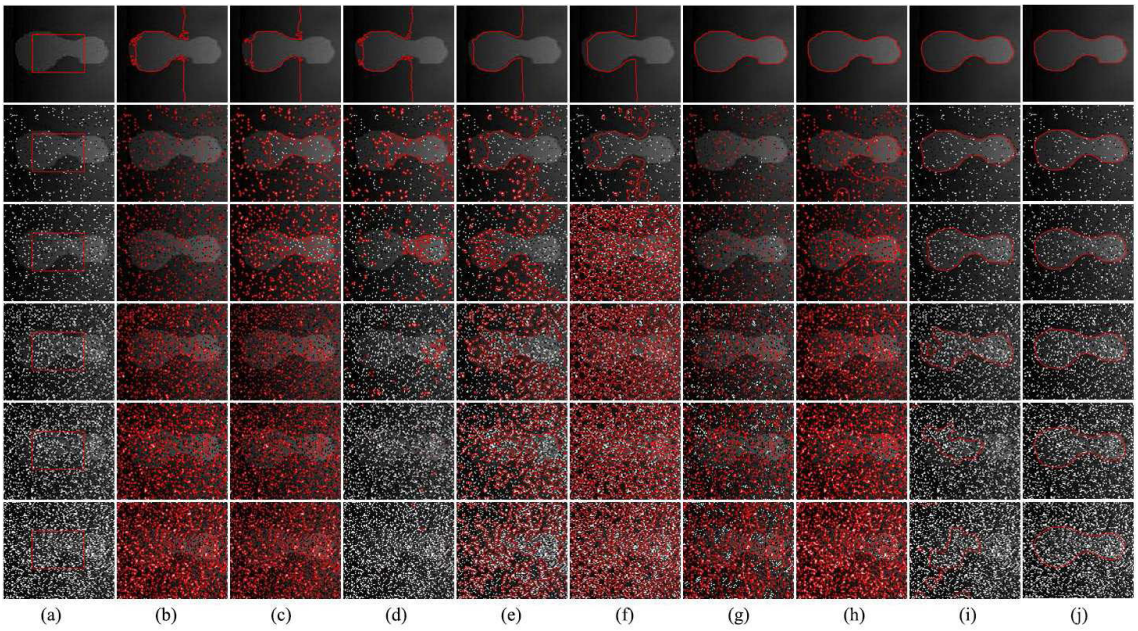

FIGURE 9. Segmentation results of the image with different levels of salt and pepper noise. (a) Images with initial contour, (b)-(j) Results of CV, SBGFRLS, ALGR, FRAGL, HLFRA, LBF, LIF, GLSEPF and the proposed model, respectively. Rows 1 to 6: Images with noise level 0, 0.05, 0.1, 0.2, 0.3, 0.4.

with GLSEF, the proposed model is more robust to the initial contour, as shown in Fig. 7.

In practice, noise and intensity inhomogeneity will degrade the quality of an image. Therefore, the following experiments are used to validate the robustness of our model to Gaussian noise and salt and pepper noise, as shown in Figs. 8 and 9. The two images are corrupted by intensity inhomogeneity. Different levels of Gaussian noise with the intensity mean of 0 and the variance of 0, 0.0005, 0.001, 0.002, 0.003 and 0.004, respectively, are added to the first T-shape image. The corresponding segmentation results of the different methods are shown in Fig. 8. Salt and pepper noise is added to the second image, the density of which is respectively set as 0, 0.05, 0.1, 0.2, 0.3 and 0.4. The segmentation results are shown in Fig. 9. We can find that the CV, SBGFRLS, ALGR, FRAGL and HLFRA methods fail to obtain desirable segmentation results. As shown in Figs. 8 and 9, LBF and LIF can correctly segment inhomogeneous images with Gaussian

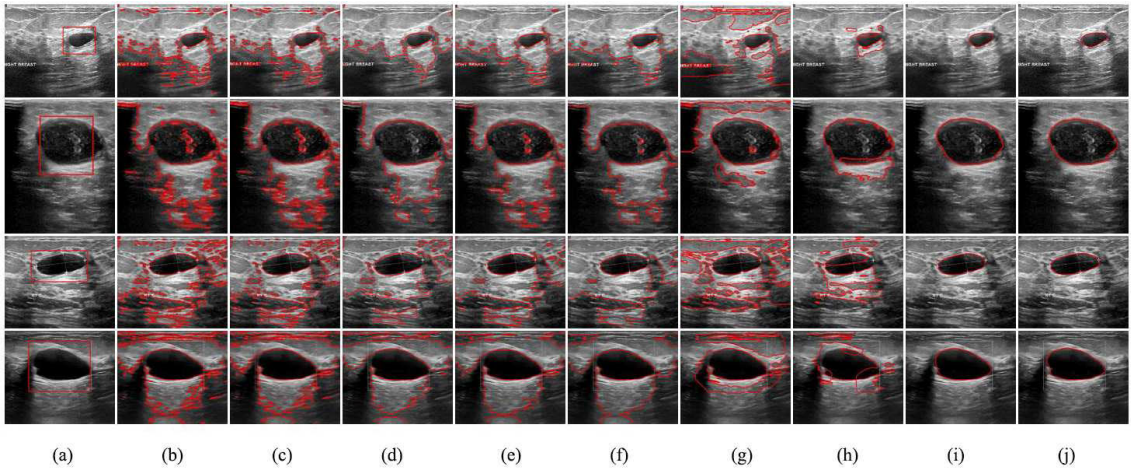

FIGURE 10. The final evolving curve for the breast ultrasound images. (a) Images with initial contour. (b)-(j) Results of CV, SBGFRLS, ALGR, FRAGL, HLFRA, LBF, LIF, GLSEPF and the proposed model, respectively.

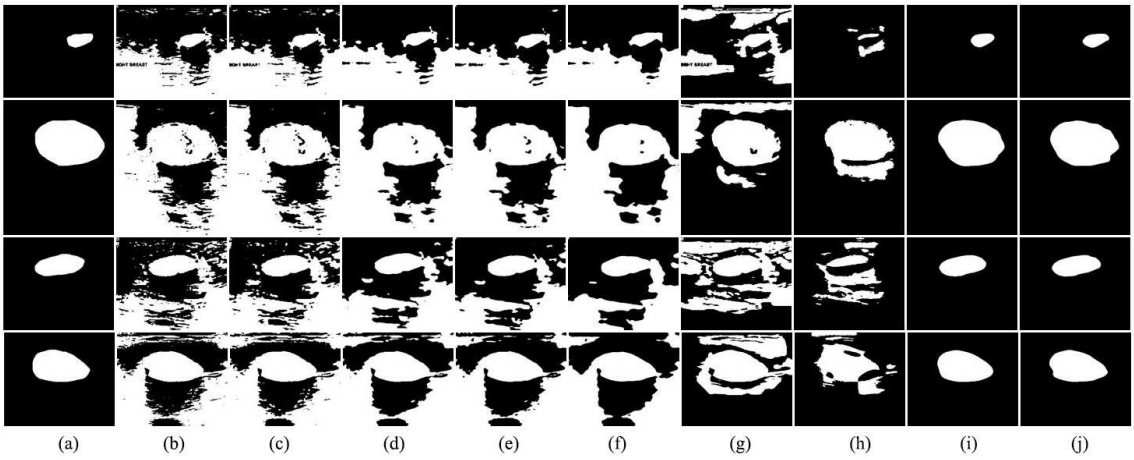

FIGURE 11. Segmentation results of the breast ultrasound images shown in Figure 10. (a) Ground truth, (b)-(j) Results of CV, SBGFRLS, ALGR, FRAGL, HLFRA, LBF, LIF, GLSEPF and the proposed model, respectively.

noise to some extent. However, they are sensitive to salt and pepper noise. By contrast, our model and GLSEPF perform better. However, our model is more robust to salt and pepper noise than GLSEPF, as shown in Fig. 9. The DSCs of all methods corresponding to Figs. 8 and 9 are listed in Table 1.

To further assess the developed model, breast ultrasound is used in the following experiment. Breast cancer is one of the most common causes of death among women worldwide [46]. The quality of the segmentation results of breast ultrasound images affects subsequent automated processing, e.g., computer-aided medical image analysis. However, breast ultrasound images usually suffer from speckle noise and intensity inhomogeneity, which make the segmentation of the traditional ACMs of these image still challenging and difficult. The segmentation results of all methods are shown in Figs. 10 and 11. It can be seen that GLSEPF and our model obtain better segmentation results than global fitting based ACMs (e.g., CV and SBGFRLS) and local fitting based ACMs (e.g., LBF and LIF). Moreover, the segmentation results of the ALGR, FRAGL and HLFRA methods are similar to those of the CV and SBGFRLS methods. The main reason may be that local information captured by these methods is insufficient to segment images with intensity inhomogeneity. The DSC values of the proposed model and other compared methods for the breast ultrasound images [43] are listed in Table 2. As can be observed, our model and GLSEPF obtain larger DSC values than those obtained by the other methods, and the DSC values of our model are slightly larger than those of the GLSEPF method. Moreover, the images in Fig. 10 are used to verify the computational times of the proposed method, the results of which are listed in Table 3. As can be seen, the proposed method requires more CPU time than required by the CV, SBGFRLS, ALGR, FRAGL, HLFRA methods. However, the runtime of our method is similar to that of the GLSEPF method and lower than that of LBF and LIF. The main reason is the that global fitting term

TABLE 1. The values of DSC of different methods for images shown in Figs. 8 and Fig. 9.

Image	CV	SBGFRLS	ALGR	FRAGL	HLFRA	LBF	LIF	GLSEPF	Ours
Row 1 in Fig. 8	0.5249	0.5284	0.5585	0.5121	0.5110	0.9795	0.9770	0.9803	**0.9829**
Row 2 in Fig. 8	0.5195	0.5273	0.5198	0.5106	0.5093	0.9772	0.9750	0.9783	**0.9803**
Row 3 in Fig. 8	0.5180	0.5250	0.5205	0.5099	0.5087	0.9766	0.9730	0.9776	**0.9789**
Row 4 in Fig. 8	0.5168	0.5216	0.5192	0.5090	0.5060	0.9750	0.9703	0.9758	**0.9765**
Row 5 in Fig. 8	0.5165	0.5214	0.5181	0.5089	0.5043	0.9728	0.9555	0.9736	**0.9744**
Row 6 in Fig. 8	0.5128	0.5198	0.5187	0.5090	0.5048	0.9655	0.9480	0.9701	**0.9732**
Row 1 in Fig. 9	0.5613	0.5576	0.5592	0.5539	0.5447	0.9844	0.9816	0.9795	**0.9856**
Row 2 in Fig. 9	0.0412	0.6328	0.5440	0.5214	0.5169	0.0402	0.3137	0.9729	**0.9845**
Row 3 in Fig. 9	0.0797	0.5563	0.4118	0.5403	0.4356	0.0659	0.3922	0.9425	**0.9823**
Row 4 in Fig. 9	0.1497	0.0300	0.0357	0.5374	0.3815	0.1439	0.3795	0.8696	**0.9785**
Row 5 in Fig. 9	0.1647	0.0612	0.0206	0.4643	0.3577	0.1505	0.2921	0.5236	**0.9717**
Row 6 in Fig. 9	0.2173	0.1303	0.0112	0.4646	0.3589	0.2599	0.3310	0.5268	**0.9626**

TABLE 2. The values of DSC of different methods for breast ultrasound images shown in Fig. 10.

Image	CV	SBGFRLS	ALGR	FRAGL	HLFRA	LBF	LIF	GLSEPF	Ours
Row 1 in Fig. 10	0.0990	0.0963	0.0996	0.0988	0.0958	0.1454	0.2574	0.9234	**0.9499**
Row 2 in Fig. 10	0.3679	0.3677	0.3694	0.3733	0.3733	0.6828	0.8027	0.9591	**0.9627**
Row 3 in Fig. 10	0.2625	0.2599	0.2803	0.2822	0.2486	0.2790	0.2778	0.9409	**0.9515**
Row 4 in Fig. 10	0.3678	0.3580	0.3708	0.3823	0.3873	0.5406	0.6549	0.9677	**0.9728**

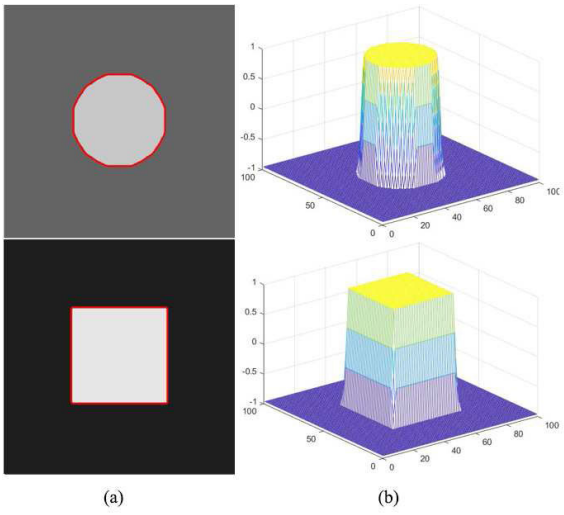

FIGURE 12. (a) Segmentation results of two binary images. (b) Corresponding *pspf*($I(x)$).

TABLE 3. Iteration and computation time (s) of the images in Fig. 10.

Image	Row 1 Iterations/Time	Row 2 Iterations/Time	Row 3 Iterations/Time	Row 4 Iterations/Time
CV	27/0.084	70/0.173	60/0.116	80/0.223
SBGFRLS	15/0.044	10/0.031	10/0.027	5/0.026
ALGR	20/0.194	20/0.184	20/0.139	25/0.221
FRAGL	10/0.159	10/0.155	10/0.139	15/0.217
HLFRA	20/0.235	10/0.129	20/0.276	15/0.206
LBF	900/6.001	1200/7.815	500/ 2.384	1000/7.820
LIF	300/3.860	200/2.284	500/4.210	400/5.708
GLSEPF	100/1.445	70/1.050	50/0.615	150/2.439
Ours	100/0.626	140/0.912	50 /0.268	170/1.355

in our model and that in the GLSEPF method can accelerate the convergence of the algorithm.

V. DISCUSSION

As shown in Fig. 5, the level set evolution of the proposed model can start with a constant function. The main reason

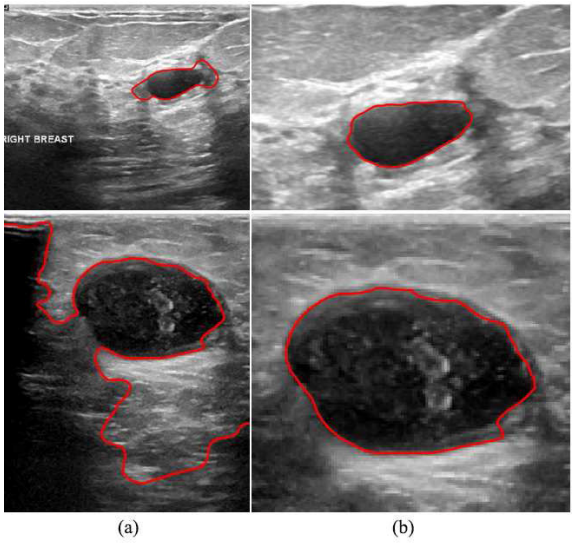

FIGURE 13. Level set evolution starts with a constant function. Segmentation results of two breast ultrasound images. (b) Segmentation results of two images cropped from (a).

is that the patch-based $psfp(I(x))$ has the following property: it has opposite signs inside and outside the object. To demonstrate this property, the LSF is initialized as a constant function, and the following equation is used to segment two binary images

$$\frac{\partial \phi}{\partial t} = pspf(I(x)) \tag{47}$$

Fig. 12(a) shows the final segmentation results. From the corresponding $psfp(I(x))$ shown in Fig. 12(b), we can easily find that the property mentioned above is satisfied. Moreover, if $pspf(I(x)) > 0$, then $\partial\phi/\partial\phi > 0$, and (47) will make ϕ increase; if $pspf(I(x)) < 0$, then $\partial\phi/\partial\phi < 0$, and (47) will make ϕ decrease. Therefore, $pspf(I(x))$ can drive the LSF ϕ

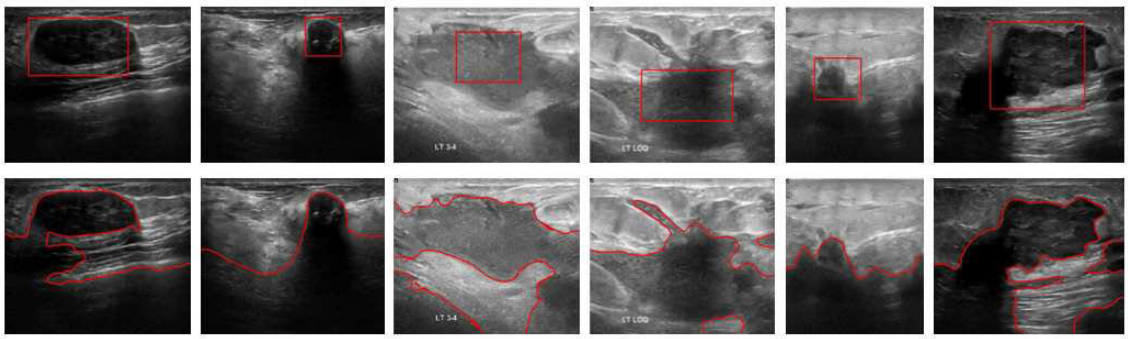

FIGURE 14. Limitation of the proposed model. Row 1: original images with initial contours. Row 2: Segmentation results of the proposed model.

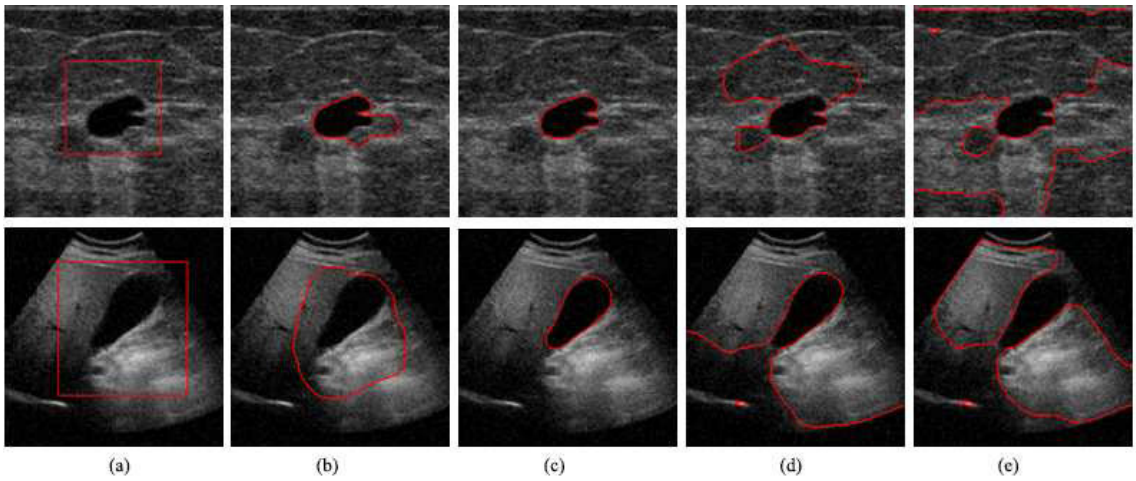

FIGURE 15. The effect of the parameter ν. (a) Original images, (b)-(e) Segmentation results by setting ν as 0, 0.05, 0.75,0.1, respectively.

to make adaptive changes, and a constant function can be used as the initialization of the contour.

Is the constant value initialization method valid for all images? To answer this question, we conduct the following experiment, as shown in Fig. 13, where the LSF is initialized as a constant function. From Fig. 13(a), we find that the segmentation results are not ideal. From rows 1 and 2 in Fig. 10(d), however, we find that the proposed model obtains desirable results when the LSFs are placed in the same image locations as those shown in rows 1 and 2 in Fig. 10(a). Moreover, the segmentation results of the images, which are a part of the original images, are as desired. Therefore, we draw the following conclusions. The developed method has greatly improved the robustness of our model to the initial contour compared with the traditional ACMs. However, the contour cannot be initialized as a constant function for all images. In addition, the proposed model dose not work well on all types of images. For example, when the intensity of the target region is similar to that of most of the background region or the boundary of the target object is very blurred, the proposed model fails to obtain desirable segmentation results, as shown in Fig. 14.

In our model, the constant parameter ν is used to control the influence of the patch-based external force term. As shown in Fig. 15, our model is utilized to segment two ultrasound images by setting different values of the parameter ν. Fig. 15(a) shows the original images, and Figs. 15(b)-(e) show the segmentation results of the proposed model for values ν of 0, 0.05, 0.075 and 0.1, respectively. When we set $\nu = 0$, the local fitting energy term is the main force driving the evolving curve, and incorrect segmentation results are obtained as shown in the second column. This demonstrates that the local fitting energy term easily becomes trapped in the local minimum. Therefore, the patch-based external force term is necessary for our model. However, when we set $\nu = 0.075$ or 0.1, our model fails to segment these ultrasound images, because the patch-based external force term will control the evolution of the curve and less information is captured. In fact, we should set the value of ν according to the level of the intensity inhomogeneity. Generally, if images suffer from severe intensity inhomogeneity, the parameter ν should be set to a small value, otherwise, it should be set to a large value. In this paper, we set $\nu = 0.05$, which is appropriate for all images.

VI. CONCLUSION

In this work, a novel active contour model is presented to segment images with noise and intensity inhomogeneity. The optimized FoE can suppress artifacts in the background and indicate the desirable edges of objects of interest. In addition, the patch-based SPF and local robust statistics make the proposed model more robust to noise and the position of the initial contour. Moreover, the JSD-based local fitting energy term can capture more information of the local robust statistics of the input image, improving the ability of the proposed model to deal with intensity inhomogeneity. The experimental results demonstrate the advantages of the proposed model over several state-of-the-art methods in terms of accuracy.

REFERENCES

[1] D. L. Pham, C. Xu, and J. L. Prince, "Current methods in medical image segmentation," *Annu. Rev. Biomed. Eng., Annu. Rev.*, vol. 2, no. 1, pp. 315–337, 2000.

[2] D. Cremers, M. Rousson, and R. Deriche, "A review of statistical approaches to level set segmentation: Integrating color, texture, motion and shape," *Int. J. Comput. Vis.*, vol. 72, no. 2, pp. 195–215, Apr. 2007.

[3] H. Lv, Z. Wang, S. Fu, C. Zhang, L. Zhai, and X. Liu, "A robust active contour segmentation based on fractional-order differentiation and fuzzy energy," *IEEE Access*, vol. 5, pp. 7753–7761, Apr. 2017.

[4] H. Lv, S. Fu, C. Zhang, and X. Liu, "Non-local weighted fuzzy energy-based active contour model with level set evolution starting with a constant function," *IET Image Process.*, vol. 13, no. 7, pp. 1115–1123, May 2019.

[5] K. Ding, L. Xiao, and G. Weng, "Active contours driven by region-scalable fitting and optimized Laplacian of Gaussian energy for image segmentation," *Signal Process.*, vol. 134, pp. 224–233, May 2017.

[6] C. Huang and L. Zeng, "Robust image segmentation using local robust statistics and correntropy-based K-means clustering," *Opt. Lasers Eng.*, vol. 66, pp. 187–203, Mar. 2015.

[7] V. Caselles, F. Catté, T. Coll, and F. Dibos, "A geometric model for active contours in image processing," *Numerische Math.*, vol. 66, no. 1, pp. 1–31, Dec. 1993.

[8] A. Khadidos, V. Sanchez, and C.-T. Li, "Weighted level set evolution based on local edge features for medical image segmentation," *IEEE Trans. Image Process.*, vol. 26, no. 4, pp. 1979–1991, Apr. 2017.

[9] C. Li, C. Xu, C. Gui, and M. D. Fox, "Distance regularized level set evolution and its application to image segmentation," *IEEE Trans. Image Process.*, vol. 19, no. 12, pp. 3243–3254, Dec. 2010.

[10] V. Caselles, R. Kimmel, and G. Sapiro, "Geodesic active contours," *Int. J. Comput. Vis.*, vol. 22, no. 1, pp. 61–79, 1997.

[11] D. Munford and J. Shah, "Optimal approximation by piecewise smooth functions and associated variational problems," *Commun. Pure Appl. Math.*, vol. 42, no. 5, pp. 577–685, Jul. 1989.

[12] T. F. Chan and L. A. Vese, "Active contours without edges," *IEEE Trans. Image Process.*, vol. 10, no. 2, pp. 266–277, Feb. 2001.

[13] K. Zhang, L. Zhang, H. Song, and W. Zhou, "Active contours with selective local or global segmentation: A new formulation and level set method," *Image Vis. Comput.*, vol. 28, no. 4, pp. 668–676, Apr. 2010.

[14] B. Han and Y. Wu, "Active contours driven by median global image fitting energy for SAR river image segmentation," *Digit. Signal Process.*, vol. 71, pp. 46–60, Dec. 2017.

[15] S. Krinidis and V. Chatzis, "Fuzzy energy-based active contours," *IEEE Trans. Image Process.*, vol. 18, no. 12, pp. 2747–2755, Dec. 2009.

[16] Y. Wu, W. Ma, M. Gong, H. Li, and L. Jiao, "Novel fuzzy active contour model with kernel metric for image segmentation," *Appl. Soft Comput.*, vol. 34, pp. 301–311, Sep. 2015.

[17] C. Li, C.-Y. Kao, J. C. Gore, and Z. Ding, "Minimization of region-scalable fitting energy for image segmentation," *IEEE Trans. Image Process.*, vol. 17, no. 10, pp. 1940–1949, Sep. 2008.

[18] C. Li, C.-Y. Kao, J. C. Gore, and Z. Ding, "Implicit active contours driven by local binary fitting energy," in *Proc. IEEE Conf. Comput. Vis. Pattern Recognit.*, Jun. 2007, pp. 1–7.

[19] K. Zhang, H. Song, and L. Zhang, "Active contours driven by local image fitting energy," *Pattern Recognit.*, vol. 43, no. 4, pp. 1199–1206, Apr. 2010.

[20] S. Liu and Y. Peng, "A local region-based Chan–Vese model for image segmentation," *Pattern Recognit.*, vol. 45, no. 7, pp. 2769–2779, Jul. 2012.

[21] L. Wang, Y. Chang, H. Wang, Z. Wu, J. Pu, and X. Yang, "An active contour model based on local fitted images for image segmentation," *Inf. Sci.*, vols. 418–419, pp. 61–73, Dec. 2017.

[22] L. Wang, L. Zhang, X. Yang, P. Yi, and H. Chen, "Level set based segmentation using local fitted images and inhomogeneity entropy," *Signal Process.*, vol. 167, Feb. 2020, Art. no. 107297.

[23] H. Lv, F. Zhang, and R. Wang, "Fuzzy active contour model using fractional-order diffusion based edge indicator and fuzzy local fitted image," *IEEE Access*, vol. 8, pp. 172707–172722, Sep. 2020.

[24] H. Ali, N. Badshah, K. Chen, and G. A. Khan, "A variational model with hybrid images data fitting energies for segmentation of images with intensity inhomogeneity," *Pattern Recognit.*, vol. 51, pp. 27–42, Mar. 2016.

[25] F. Akram, M. A. Garcia, and D. Puig, "Active contours driven by local and global fitted image models for image segmentation robust to intensity inhomogeneity," *PLoS ONE*, vol. 12, no. 4, Apr. 2017, Art. no. e0174813.

[26] B. Han and Y. Wu, "Active contours driven by global and local weighted signed pressure force for image segmentation," *Pattern Recognit.*, vol. 88, pp. 715–728, Apr. 2019.

[27] J. Fang, H. Liu, L. Zhang, J. Liu, and H. Liu, "Active contour driven by weighted hybrid signed pressure force for image segmentation," *IEEE Access*, vol. 7, pp. 97492–97504, Jul. 2019.

[28] H. Liu, J. Fang, Z. Zhang, and Y. Lin, "A novel active contour model guided by global and local signed energy-based pressure force," *IEEE Access*, vol. 8, pp. 59412–59426, Mar. 2020.

[29] X. Yang, X. Jiang, L. Zhou, Y. Wang, and Y. Zhang, "Active contours driven by local and global region-based information for image segmentation," *IEEE Access*, vol. 8, pp. 6460–6470, Jan. 2020.

[30] J. Fang, H. Liu, L. Zhang, J. Liu, and H. Liu, "Fuzzy region-based active contours driven by weighting global and local fitting energy," *IEEE Access*, vol. 7, pp. 184518–184536, Apr. 2019.

[31] J. Fang, H. Liu, L. Zhang, J. Liu, and H. Liu, "Region-edge-based active contours driven by hybrid and local fuzzy region-based energy for image segmentation," *Inf. Sci.*, vol. 546, pp. 397–419, Feb. 2021.

[32] L. Fang, T. Qiu, H. Zhao, and F. Lv, "A hybrid active contour model based on global and local information for medical image segmentation," *Multidimensional Syst. Signal Process.*, vol. 30, no. 2, pp. 689–703, Apr. 2019.

[33] X. F. Wang, D. S. Huang, and H. Xu, "An efficient local Chan-Vese model for image segmentation," *Pattern Recognit.*, vol. 43, no. 3, pp. 603–618, Mar. 2010.

[34] M. M. Abdelsamea and G. Gnecco, "Robust local–global SOM-based ACM," *Electron. Lett.*, vol. 51, no. 2, pp. 142–143, Jan. 2015.

[35] L. Sun, X. Meng, J. Xu, and Y. Tian, "An image segmentation method using an active contour model based on improved SPF and LIF," *Appl. Sci.*, vol. 8, no. 12, p. 2576, Dec. 2018.

[36] S. Zhou, J. Wang, S. Zhang, Y. Liang, and Y. Gong, "Active contour model based on local and global intensity information for medical image segmentation," *Neurocomputing*, vol. 186, pp. 107–118, Apr. 2016.

[37] Y. Gao, R. Kikinis, S. Bouix, M. Shenton, and A. Tannenbaum, "A 3D interactive multi-object segmentation tool using local robust statistics driven active contours," *Med. Image Anal.*, vol. 16, no. 6, pp. 1216–1227, Aug. 2012.

[38] J. M. Cruz–Duarte, J. Rosales–Garcia, C. R. Correa–Cely, A. Garcia–Perez, and J. G. Avina–Cervantes, "A closed form expression for the Gaussian–based Caputo–Fabrizio fractional derivative for signal processing applications," *Commun. Nonlinear Sci. Numer. Simul.*, vol. 61, pp. 138–148, Aug. 2018.

[39] G. Zhang, J. Liu, J. Wang, Z. Tang, Y. Xie, J. He, T. Ma, and J. P. Niyoyita, "FoGDbED: Fractional-order Gaussian derivatives-based edge-relevant structure detection using Caputo-Fabrizio definition," *Digit. Signal Process.*, vol. 98, Mar. 2020, Art. no. 102639.

[40] M. Caputo and M. Frabrizio, "A new definition of fractional derivative without singular kernel," *Prog. Fract. Differ. Appl.*, vol. 1, no. 2, pp. 73–85, 2015.

[41] M. M. Abdelsamea, A. Pitiot, R. B. Grineviciute, J. Besusparis, A. Laurinavicius, and M. Ilyas, "A cascade-learning approach for automated segmentation of tumour epithelium in colorectal cancer," *Expert Syst. Appl.*, vol. 118, pp. 539–552, Mar. 2019.

[42] L. Xu, Y. Zhu, Y. Zhang, and H. Yang, "Liver segmentation based on region growing and level set active contour model with new signed pressure force function," *Optik*, vol. 202, Feb. 2020, Art. no. 163705.
[43] Z. Ji, Y. Xia, Q. Chen, Q. Sun, D. Xia, and D.-D. Feng, "Fuzzy C-means clustering with weighted image patch for image segmentation," *Appl. Soft. Comput.*, vol. 12, no. 6, pp. 1667–16959, Jun. 2012.
[44] B. Han and Y. Wu, "Active contour model for inhomogenous image segmentation based on Jeffreys divergence," *Pattern Recognit.*, vol. 107, Nov. 2020, Art. no. 107520.
[45] F. Nielsen, "On the Jensen–Shannon symmetrization of distances relying on abstract means," *Entropy*, vol. 21, no. 5, p. 485, May 2019.
[46] W. Al-Dhabyani, M. Gomaa, H. Khaled, and A. Fahmy, "Dataset of breast ultrasound images," *Data Brief*, vol. 28, Feb. 2020, Art. no. 104863.

HONGLI LV received the B.S. degree from the School of Mathematics and Statistics, Henan University, Kaifeng, China, in 2007, the M.S. degree from the College of Mathematics and Information Science, Wenzhou University, Wenzhou, China, in 2015, and the Ph.D. degree in computational mathematics from Shandong University, in 2018. He is currently a University Lecturer with the School of Information Technology, Shangqiu Normal University, and a Research Associate with the College of Big Data and Software Engineering, Zhejiang Wanli University. His research interests include medical image processing and computer vision, especially image denoising and image segmentation.

FANGJIAN ZHANG received the B.S. degree from Shangqiu Normal University, Shangqiu, China, in 2006. He is currently a Senior Research Assistant with the School of Information Technology, Shangqiu Normal University. His research interests include image processing, multimedia processing technology, and intelligence computation.

RENFANG WANG received the Ph.D. degree from the State Key Laboratory of CAD & CG, Zhejiang University. He is currently a Professor with the College of Big Data and Software Engineering, Zhejiang Wanli University. He is the third level of 151 Talent Project in Zhejiang Province and the second level of Leading Talents in Ningbo. His research interests include computer graphics, image processing, and multimedia processing technology.